Incorporating EEG and fNIRS Patterns to Evaluate Cortical Excitability and MI-BCI Performance During Motor Training

Zhongpeng Wang, *Member, IEEE*, Lu Yang, Yijie Zhou, Long Chen, Bin Gu, Shuang Liu, Minpeng Xu, *Senior Member, IEEE*, Feng He, and Dong Ming, *Senior Member, IEEE*

***Abstract*— As electroencephalography (EEG) is nonlinear and nonstationary in nature, an imperative challenge for brain-computer interfaces (BCIs) is to construct a robust classifier that can survive for a long time and monitor the brain state stably. To this end, this research aims to improve BCI performance by incorporation of electroencephalographic and cerebral hemodynamic patterns. A motor imagery (MI)-BCI based visual-haptic neurofeedback training (NFT) experiment was designed with sixteen participants. EEG and functional near infrared spectroscopy (fNIRS) signals were simultaneously recorded before and after this transient NFT. Cortical activation was significantly improved after repeated and continuous NFT through time-frequency and topological analysis. A classifier calibration strategy, weighted EEG-fNIRS patterns (WENP), was proposed, in which elementary classifiers were constructed by using both the EEG and fNIRS information and then integrated into a strong classifier with their independent accuracy-based weight assessment. The results revealed that the classifier constructed on integrating EEG and fNIRS patterns was significantly superior to that only with independent information (∼10% and ∼18% improvement respectively), reaching ∼89% in mean classification accuracy. The WENP is a classifier calibration strategy that can effectively improve the performance of the MI-BCI and could also be used to other BCI paradigms. These findings validate that our proposed methods are feasible and promising for optimizing conventional motor training methods and clinical rehabilitation.**

***Index Terms*— Brain–computer interface, neurofeedback training, hybrid brain signal, weighted EEG-fNIRS patterns, motor imagery.**

Manuscript received 30 January 2023; revised 9 May 2023; accepted 26 May 2023. Date of publication 1 June 2023; date of current version 10 July 2023. This work was supported in part by the National Key Research and Development Program of China under Grant 2022YFF1202304; in part by the National Natural Science Foundation of China under Grant 62006171, Grant 82001939, and Grant 81925020; and in part by the Natural Science Foundation of Tianjin under Grant 22JCYBJC01430. *(Corresponding authors: Long Chen; Dong Ming.)*

This work involved human subjects or animals in its research. Approval of all ethical and experimental procedures and protocols was granted by the Ethics Committee of Tianjin University under Approval No. TJUE-2020-056.

Zhongpeng Wang, Bin Gu, Minpeng Xu, Feng He, and Dong Ming are with the Academy of Medical Engineering and Translational Medicine, the College of Precision Instruments and Optoelectronics Engineering, the Tianjin Center for Brain Science, and the Tianjin International Joint Research Center for Neural Engineering, Tianjin University, Tianjin 300072, China (e-mail: richardming@tju.edu.cn).

Lu Yang, Yijie Zhou, Long Chen, and Shuang Liu are with the Academy of Medical Engineering and Translational Medicine, Tianjin University, Tianjin 300072, China (e-mail: cagor@tju.edu.cn).

Digital Object Identifier 10.1109/TNSRE.2023.3281855

I. Introduction

BRAIN–COMPUTER interfaces (BCIs) can provide instantaneous and quantitative measures of cerebral functions modulated by motor imagery (MI), which is assumed to enhance the efficiency of motor recovery [1], as MI-BCI technology can directly decode brain central nervous system (CNS) motor information and build a brain machine feedback loop to assist motor rehabilitation training [2]. Based on the central nervous system plasticity theory, MI-BCI opened up a new pathway for motor imagery therapy in the clinical application of brain nerve rehabilitation [3], [4], [5].

More importantly, BCI can provide quantitative and observable measures of cerebral functions modulated by MI. Therfore, the active participation of patients can be well observed and promoted in the MI-BCI feedback system, and MI-BCI can provide strict control and instantaneous regulation of target training for patients and clinical physicians [6]. MI-BCI combining functional electrical stimulation (FES) has become a more effective approach than traditional FES therapy for stroke rehabilitation [7]. Many modeling and recognition optimization methods of MI-BCI systems have been proposed in many studies [8], [9]. In addition, functional changes for neural reorganization induced by BCI and its evaluation have become a new research focus [10], [11], [12].

It is difficult to discard the calibration phase, thereby increasing the time cost of motor rehabilitation training [13], [14]. Brain waves decoding based on electroencephalography (EEG) can transmit the prompt and objective information about the neuro-cortical activations to the outside world [15], [16]. Although EEG-based BCI enables some paralyzed patients to interact with the outside world, functional near-infrared spectroscopy (fNIRS) might be a feasible monitoring method combined with a classical conditioning paradigm for locked-in syndrome [17], [18], [19]. Single-mode

brain functional imaging techniques are limited. Therefore, through a variety of functional brain imaging technologies, multiple measurement methods can be realized to reflect the brain activation situation synchronously, and the information among various brain signals can supplement each other to obtain better measurement accuracy and brain function. Therefore, simultaneous measurement of fNIRS and EEG is widely used in neuroimaging studies [20], [21], [22].

According to previous studies, the complex correlations between brain structures, function and electrophysiological patterns could be probed and clarified by incorporation of different brain signals [23], [24], [25]. As an independent signal mode provides a partial monitor and assessment of neural activations, the incorporation of EEG and fNIRS might provide a feasible analysis for comprehensive brain response and its dynamic measurement and assessment. There have been many categories and methods of joint EEG-fNIRS analyses, which can be divided into asymmetric and symmetric. More of these techniques can indeed provide additional insights and complementary information by multidata fusion, especially in BCIs [26], [27], [28], [29], [30]. Fazli et al. attempted to design a new BCI training paradigm using the combined signal detection method of EEG-fNIRS. The results showed that EEG combined with fNIRS significantly improved the accuracy of MI classification in more than 90% of subjects and improved performance by an average of 5% [31]. Buccino et al. further combined EEG and fNIRS to distinguish four types of action execution tasks, and improved the distinguishing ability of the overall neural response characteristics by optimizing the filtering algorithm and overcoming the time-delay problem of fNIRS haemodynamic response [32]. However, due to the complexity of neurovascular coupling [33], these methods are not mature.

This study proposed the incorporation of EEG and fNIRS to improve MI-based BCI classification performance. We have demonstrated that an EEG-based visual-haptic paradigm could enhance cortical activations and classification accuracy [34]. Additionally, EEG and fNIRS signals were recorded synchronously so that the Graz MI-BCI paradigm was used to explore the changes in MI-induced EEG and fNIRS patterns. We assessed cortical excitability and compared different fusion methods of hybrid brain signals to optimize MI-based BCI performance.

II. Methods

A. Subjects

This study was undertaken at the Neural Engineering and Rehabilitation Laboratory of Tianjin University. The ethical committee of Tianjin University approved all of this experimental study. Nineteen healthy and right-handed participants (7 females and 12 males, age range 21–28 years old, mean±std.: 24.2 ± 2.3) took part in the study. They had no history of neurological or psychiatric disorders. The experimental procedure was clearly explained to each participant, and written informed consent was also signed before data recording. Sixteen out of the nineteen subjects participated in EEG-fNIRS joint acquisition because of the upgrade of the experimental acquisition equipment.

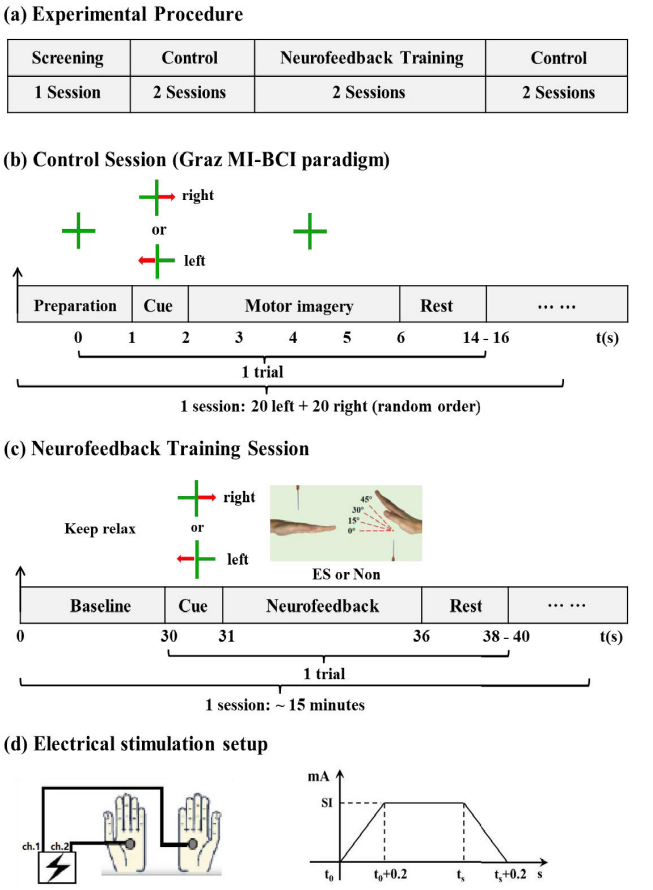

Fig. 1. Setup of experimental paradigm. (a) Procedure and sessions. Paradigms and timing of (b) Previous and posterior control sessions using Graz MI-BCI paradigm, (c) NFT sessions. (d) Electrical stimulation. SI indicates stimulation intensity of all subjects individually determined.

B. Experimental Paradigm

Our previous work has described this experimental paradigm in detail but no EEG-fNIRS joint acquisition [34]. As shown in Fig. 1, the experiment was separated into four task conditions (one screening session, two previous control sessions, two NFT sessions and two posterior control sessions). First, all subjects could have a screening session at the beginning, including all of the experimental paradigms. Two previous control sessions implemented the common Graz MI-BCI paradigm [35], [36]. Each session contained 40 trials of left or right hand MI, and more details were shown in Fig. 1(b). However, each trial contained a relatively long random rest time of 8 to 10 s, ensuring the integrity and synchronization of MI-induced EEG and fNIRS pattern changes. During the next 30 minutes, two visual-haptic NFT sessions were conducted for all subjects. Considering the comfort of human wrist movement, 0°, 15°, 30° and 45° were selected as the angle range for the virtual hand. The angle range of the virtual hand was used for visual representation and real-time feedback of NFT characteristic parameter level. The corresponding relationship between them was detailed in previous research [34]. According to the NFT parameters, the two virtual hands placed in the middle of the screen approach or move away from the needles once a second. Once the needle

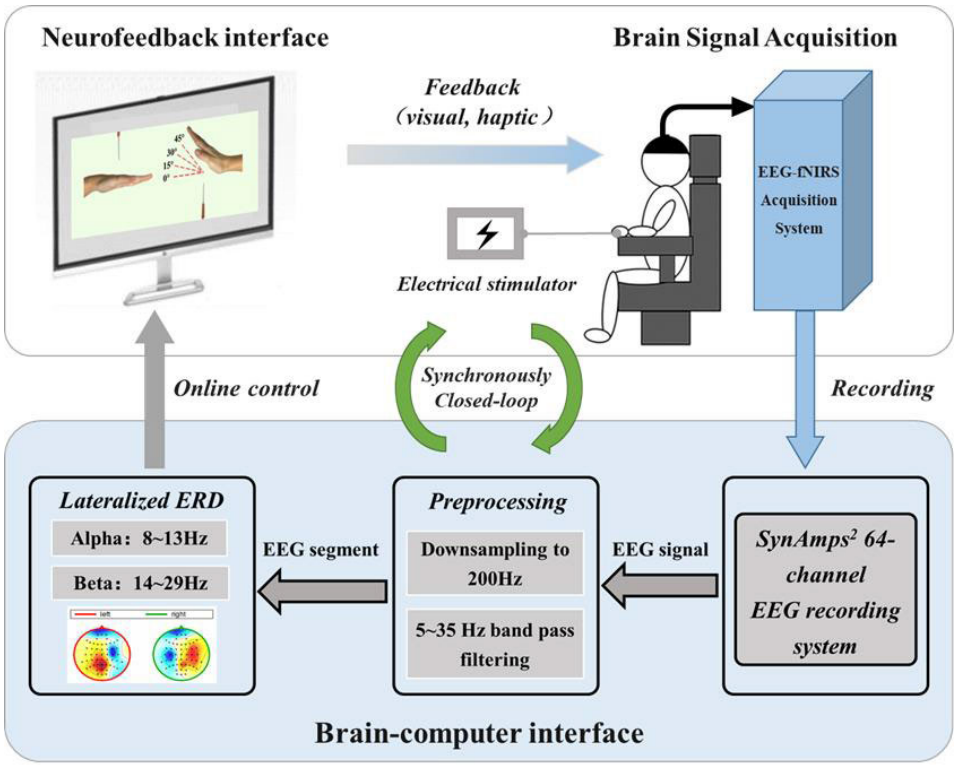

Fig. 2. Experimental system by BCI-based visual-haptic NFT [29].

touches the hand (t_0), there would be an electrical stimulation (ES) as shown in Fig. 1(d) applying to left and right hand palms of the subject until the needle move away from the hand or this trial ends (t_s). Posterior control sessions were also implemented using the same Graz MI-BCI paradigm. All subjects should apply the kinesthetic MI strategy that has been repeatedly trained and optimized during NFT sessions.

As shown in Fig. 2, a BCI system translates EEG activities by feature extraction and recognition to control external devices and thereby changes the ongoing neurofeedback interface and electrical stimulator, achieving the effect and process of NFT. In our typical EEG-BCI-based visual-haptic NFT, left- or right-hand movement intention could be decoded in real time during NFT by extracting MI-induced EEG features. The effectiveness of MI detection would trigger feedback every 1 s. This feedback could also be delivered in a visual hands movement display on the computer screen and haptic stimulation by the electrical stimulator that reproduces and promotes the intended movement. All subjects were asked to imagine haptic sensation, force, or position of squeezing an object such as a cup or ball, but not its scene in the mind). Theoretically, during such transient and repetitive NFT, better kinesthetic MI should generate stronger sensorimotor cortical excitability and higher classification performance [35], [36].

C. Hybrid Brain-Signal Acquisition and Preprocessing

The scalp EEGs were recorded with a SynAmps2 amplifier (Neuroscan, Australia) and 64-channel Quik-Cap (standard Ag/AgCl electrodes) according to the international 10-20 system. The sampling rate was set to 1000 Hz with band-pass filtering between 0.05 and 100 Hz and a 50 Hz notch. The reference and ground electrodes were placed on the nose and forehead, respectively. Before data acquisition, the impedance of all electrodes was kept below 10 kΩ. For preprocessing, the EEG raw data were downsampled to 200 Hz, and a common average reference (CAR) was performed.

The fNIRS acquisition system synchronously recorded hemodynamics-related cerebral blood oxygen (NirScan, Danyang Huichuang Medical Equipment Co., Ltd., China). Sampling rate was set to 10 Hz. Band-pass filtering was set between 0.01 and 3 Hz. The distance between sources and detectors was 3 cm. For preprocessing, the band-pass filter was set between 0.01 and 0.2 Hz, and the classical negative correlation method for measuring cerebral blood oxygenation / deoxygenation ([oxy-Hb] / [deoxy-Hb]) hemoglobin concentration information was used to optimize fNIRS data.

As shown in Fig. 3, fNIRS channels cover the left and right sensorimotor regions. During left and right limb MI (LH-MI and RH-MI), these regions of interest (ROIs) could represent changes in the concentration of cerebral blood oxygen. In addition, we calculated time course analysis (TCA) curves, following the coherence averaging method of event-related potentials (ERPs) in EEG analysis, i.e., taking event labels as synchronization criteria to segment time data of concentration changes of [oxy-Hb] and [deoxy-Hb].

It is demonstrated by adding average repeated cerebral blood oxygen data. The mean variation in cerebral oxygen concentration during specific tasks with time was shown, and the hemodynamic response of the cerebral cortex was evaluated. To quantify and compare the difference in cerebral blood oxygen response under different training conditions and

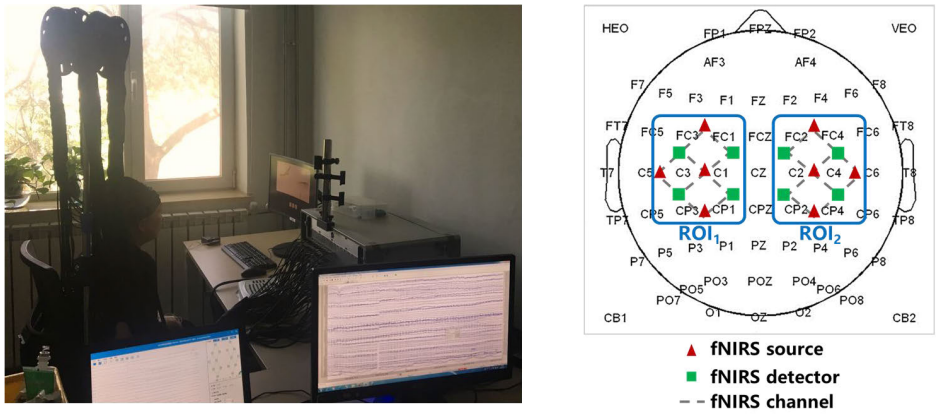

Fig. 3. Experimental equipment and scene (a) EEG-fNIRS experimental situation and equipment, (b) channel positions of hybrid brain-signal acquisition.

to characterize the activation of cerebral hemodynamics, two key cerebral blood oxygen peaks (peak amplitude) and integral areas of ROIs (ROI_1 and ROI_2) were extracted for left- and right-hand MI tasks before and after training. We applied the general linear mode (GLM) to analyze the activation state of hemodynamics in ROIs during the LH-MI and RH-MI tasks before and after training and to calculate its functional topology map based on cerebral blood oxygen characteristics.

Electrical stimulation was achieved by 2-channel VitalStim therapy equipment (Chattanooga Group, TN, USA). Its biphasic current pulse and frequency were set to 300 μs duration and 30 Hz. The ECG self-adhesive electrodes were placed on the palm and back of the left and right hands.

D. Calculation of the ERD Power and BCI Performance

In this study, EEG-based ERD power was determined as the decrease ratio of the alpha- and beta-band (8–13 Hz and 14-29 Hz) activities during MI to that during rest. We calculated the left- and right-hand MI-induced ERD powers during NFT sessions using the event-related spectral perturbation (ERSP) method:

$$\text{ERD power} = \frac{P_{task} - P_{rest}}{P_{rest}} \times 100[\%] \tag{1}$$

where P_{rest} in eq. (1) corresponds to the alpha- or beta-band short-time Fourier transform (STFT) spectrum power superposition averaged during 1 s rest period, i.e., before the MI cue (presentation of a green fixation cross in Fig. 1(b)). In the control sessions, the alpha- or beta-band activity during MI (P_{task}) was also determined as the corresponding STFT spectrum power superposition averaged every 1 s immediately after the MI cue. In addition, we also calculated the left- and right-hand MI-induced absolute ERD powers in the control sessions, which could probe cortical excitability before and after NFT sessions, respectively.

E. Weighted EEG-fNIRS Patterns (WENP)

We used common spatial patterns (CSPs) to perform a subject-dependent and supervised decomposition that enhances the discriminability between LH- and RH-MI. In our study, EEG recording channels were set N=64. CSP could output spatial filters W. Its components in one category with maximum variance for $C1$ and minimum variance for $C2$. Moreover, the other category are the opposite, with maximum variance for $C2$ and minimum for $C1$.

$$x_{CSP}(t) = W^T x(t), x_{CSP}(t) \in \mathbb{R}^{\mathrm{N}} \tag{2}$$

where $x_{CSP}(t) \in \mathbb{R}$ is the spatial filter bank and N=64 is the number of EEG measurement channels, as mentioned above. We could simultaneously diagonalize two kinds of covariance matrices (S_{C1} and S_{C2}) to assess and obtain optimal spatial filters:

$$\begin{cases} W^T S_{C1} W = A_{C1} \\ W^T S_{C2} W = A_{C2} \end{cases} \tag{3}$$

where A_{C1} and A_{C2} are diagonal matrices containing the eigenvalues. $A_{C1} + A_{C2} = I$, so that signals belonging to $C1$ have maximum variance on the first components of W and minimum variance when projected on its last components. In contrast, signals of class $C2$ have the opposite behavior.

After CSP processing, a radial basis function (RBF) kernel support vector machine (SVM) classifier was executed on existing CSP features from EEG or fNIRS data. It has been proved that SVM has relatively high classification performance using the LIBSVM toolbox [34], [37]. For subsequent use, we could obtain different classification decisions and accuracies of EEG and fNIRS.

We further explored the BCI performance under different conditions, including individual EEG or fNIRS classification analysis, EEG-fNIRS feature fusion and decision level fusion (i.e., weighted EEG-fNIRS patterns). This process could indicate its effectiveness in controlling an MI-based BCI system. As mentioned above, all features are extracted by CSP from EEG and fNIRS. In addition, then, we could get the fusion feature Z:

$$Z = F(X_i, Y_i) = \{x_1, x_2, \cdots x_m, y_1, y_2, \cdots y_n\} \tag{4}$$

$$X_i = \{x_1, x_2, \cdots x_m\} \tag{5}$$

$$Y_j = \{y_1, y_2, \cdots y_n\} \tag{6}$$

where X_i is the ith CSP feature vector from EEG data and Y_j is the jth CSP feature vector from fNIRS data. m and n are their feature vector dimensions. F is a simple feature fusion by splicing all EEG and fNIRS CSP feature vectors. According to Z inputting to SVM, we could calculate new classification accuracy by leave-one validation method. This is a linear feature fusion method commonly used in machine learning or pattern recognition.

We further calculated classification accuracies based on CSP and SVM classifier decision fusion to probe the effectiveness of performance improvement under an MI-based BCI system. Decision level fusion (i.e., WENP) is a way to integrate the decision results of various data modes, in which all primary classifiers are constructed by using both the EEG and fNIRS information. Then, we integrated these patterns into a strong classifier with their independent accuracy-based weight assessment. Each data point performs preprocessing, pattern extraction and classification as mentioned above to obtain sub-decisions. The final decision result is calculated according to the weight assessment of sub-decisions. Weight assessment from independent classification performance could theoretically effectively reduce or even eliminate the influence of incorrect sub-decisions.

Fig. 4 shows the classification calculation process based on EEG-fNIRS decision fusion. First, we perform CSP and SVM as mentioned above. It outputs accuracy (acc_{EEG}, acc_{fNIRS}) and decision value (dv_{EEG}, dv_{fNIRS}). We take accuracy as a weight (w) assessment to construct a decision fusion mode, as shown in eq. (7), and perform correlation and fusion according to both EEG and fNIRS decisions, then compare with test labels, to obtain final decision output and classification accuracy. Among them, the leave-one validation method is still used to calculate the classification accuracy, and each subject gets a classification accuracy.

$$dv_{fusion} = acc_{EEG} * w_{EEG} + acc_{fNIRS} * w_{fNIRS} \quad (7)$$

$$w_{EEG} = dv_{EEG}, w_{fNIRS} = dv_{fNIRS} \quad (8)$$

F. Statistical Analysis

We compared ERD patterns, fNIRS patterns and classification accuracy and applied paired-samples t test to all healthy subjects who participated in EEG-fNIRS joint acquisition (n= 16) for statistical analysis. The same pattern parameters from every subject before or after motor neurofeedback training can be used as paired samples. We applied one-way repeated measures analysis of variance (ANOVA) to explore the performance of MI-BCI classification, with the motor training conditions as a within-subject variable and classification accuracy as the dependent variable. The statistical analysis was performed by using SPSS 22.0 (IBM SPSS Inc., Chicago, IL, USA).

III. Results and Analysis

A. EEG Based ERSP Patterns Analysis

As shown in Fig. 5(a), to investigate MI-induced cortical excitability of control sessions before and after NFT, the average topographical distribution maps of absolute ERD powers were calculated and shown across all subjects at alpha and beta

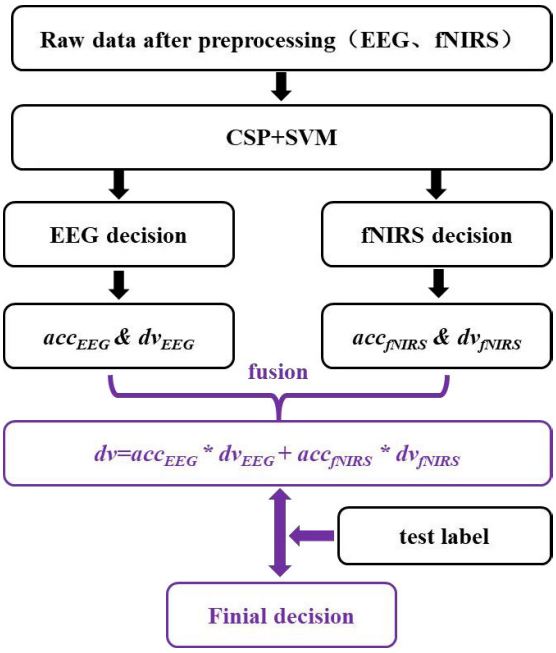

Fig. 4. Framework schematic of decision level fusion (i.e. WENP) under different data.

(8-13 Hz and 14-29 Hz) bands, two salient frequency bands. In addition, topographical maps of H-values in paired-samples t test (1 or 0 indicates $p < 0.01$ or not) could also present significant differences at the same alpha- and beta-band as above. Contralateral dominance covering sensorimotor cortical areas could be observed more clearly for posterior control sessions. Moreover, alpha- and beta-band were also selected to compare their absolute ERD powers between previous and posterior control sessions. As shown in Fig. 5(b), the average absolute alpha- and beta-ERD powers are present under the LH-MI and RH-MI tasks across all subjects, from the difference of the C3 and C4 channels (To facilitate comparison, the ERD difference of left-hand MI C4-C3, and right-hand MI in alpha and beta is C3-C4. Therefore, the average ERD in both left and right-hand MI are all the negative values.). After the Shapiro-Wilk test of normality, the paired-samples t test yielded significant differences between previous and posterior control sessions, given their statistics, significance and effect values (pre vs. post at beta-ERD of LH-MI: $t(15) = 2.347$, $p = 0.033$, $d = 0.59$; alpha-ERD of RH-MI: $t(15) = 3.661$, $p = 0.002$, $d = 0.92$). These results are relatively consistent with topographical phenomena. Therefore, the lateralized cortical excitability during MI was significantly improved after the transient NFT.

B. fNIRS Based Concentrations of Cerebral Blood Oxygen

According to the fNIRS channel positions in Fig. 3(b), it covers right- and left-hand related sensorimotor regions (ROI_1 and ROI_2). fNIRS concentration changes effectively reflect brain activation during transient neurofeedback training. Fig. 6 shows the group average time-course waveform for two fNIRS ROIs according to different MI tasks (LH-MI and RH-MI). The time-course wave represents the change

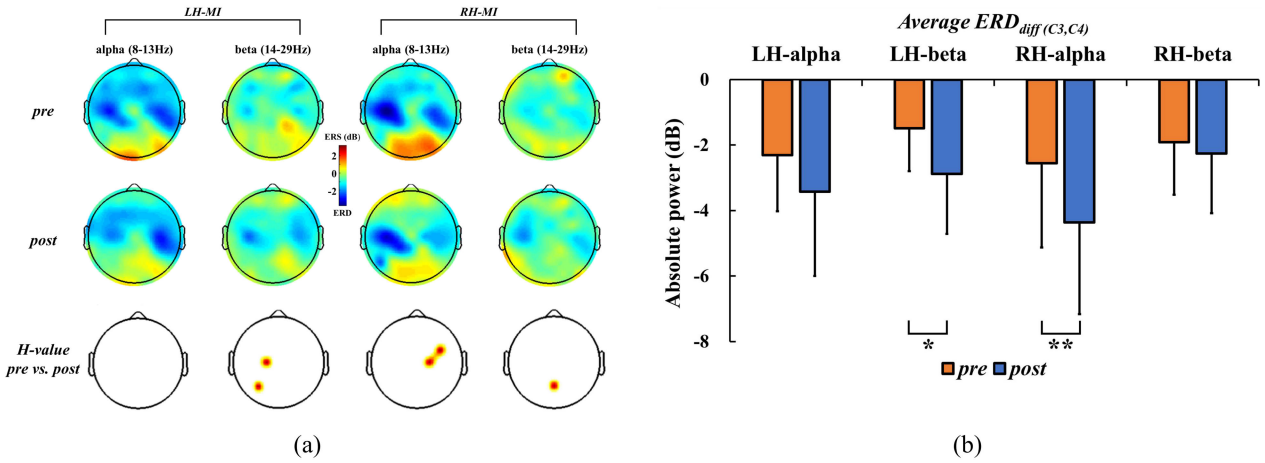

Fig. 5. ERSP patterns. (a) Topographic maps of alpha- and beta-band (8-13 Hz and 14-29 Hz) absolute ERD powers under LH- and RH-MI and their H-values (0 or 1) of paired-samples t test. The deep red indicates the distribution of significant differences after multiple comparisons (1 or 0 indicates $p < 0.01$ or not). (b) The absolute ERD powers during previous and posterior control sessions (* represents the significant difference, $^{*}p < 0.01$ and $^{**}p < 0.001$, with Shapiro-Wilk test of normality).

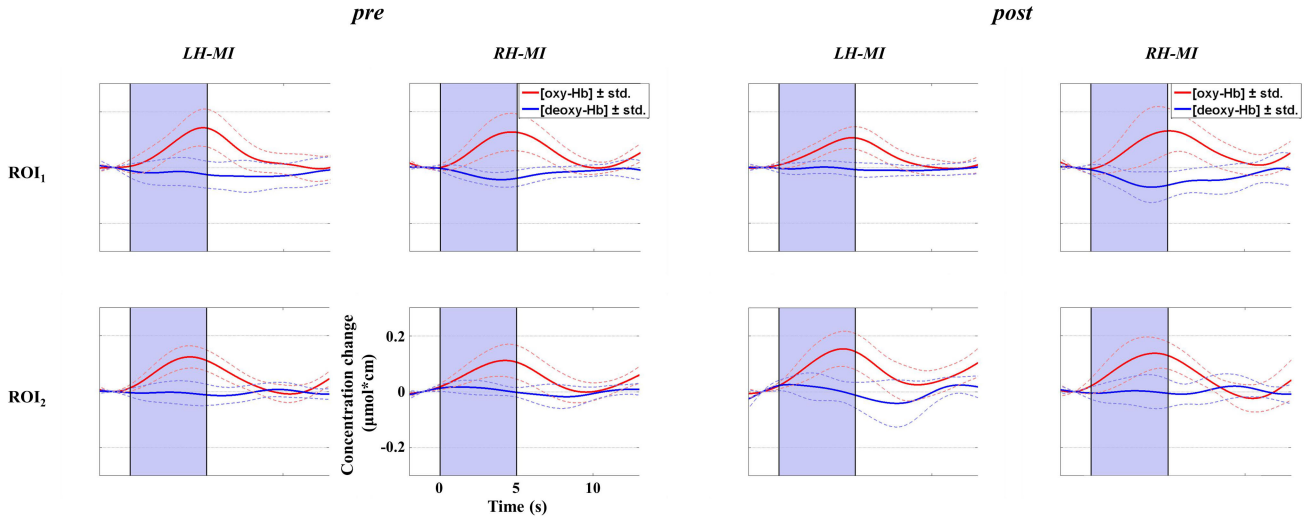

Fig. 6. The cerebral blood oxygen concentration changes before and after left- and right-hand MI-based NFT. The red curve represents the change in [oxy-Hb]. The blue curve represents the change in [deoxy-Hb] concentration. The thin dotted line of the corresponding color represents the standard error. All subgraphs use the same scale as those in the 2nd row and 2nd column subgraph.

in cerebral blood oxygen concentration. Additionally, peak amplitude and integral area differences between ROI_1 and ROI_2 were extracted under the contralateral dominance principle. These results could quantitatively show brain activation during different MI tasks before and after NFT.

As shown in Fig. 6, the hemodynamic responses had a consistent trend change, similar to EEG time-frequency analysis. After neurofeedback training, the cerebral blood oxygen response shows an obvious enhancement, especially contralateral dominance. Specifically, the cerebral blood oxygen responses of ROI_1 and ROI_2 were almost at the same level before NFT. However, right-hand MI has contralateral dominance, and its cerebral blood oxygen response level of ROI_1 is higher than that of ROI_2. After NFT sessions, both left- and right-hand MI presented significant contralateral dominance, and left-hand MI especially improved significantly. At the beginning of the task, cerebral blood oxygen concentrations had consistent changes (i.e., [oxy-Hb] wave curves first ascend during the task period and then descend to the baseline during the rest period.) which is consistent with the basic regular pattern of the cerebral blood oxygen response induced by motor-related tasks.

As shown in Fig. 7, from pattern parameter extraction and comparison analysis, cerebral blood oxygen levels induced by left- and right-hand MI improved significantly after NFT. Especially compared before and after training (*pre vs. post*), the cerebral oxygen response level induced by left-hand MI increased significantly ([oxy-Hb] peak amplitude: $t(15) = -5.057$, $p = 0.000$, $d = -1.26$; [deoxy-Hb] peak amplitude: $t(15) = 3.488$, $p = 0.003$, $d = 0.87$; [oxy-Hb] integral area: $t(15) = -3.833$, $p = 0.002$, $d = -0.96$; [deoxy-Hb] integral area: $t(15) = 3.152$, $p = 0.007$, $d = 0.79$).

C. Topological Analysis of Cerebral Hemodynamic Response

According to the regions of interest of fNIRS channel settings (ROI_1 and ROI_2), we plotted the average cerebral blood oxygen response topology of all subjects and compared

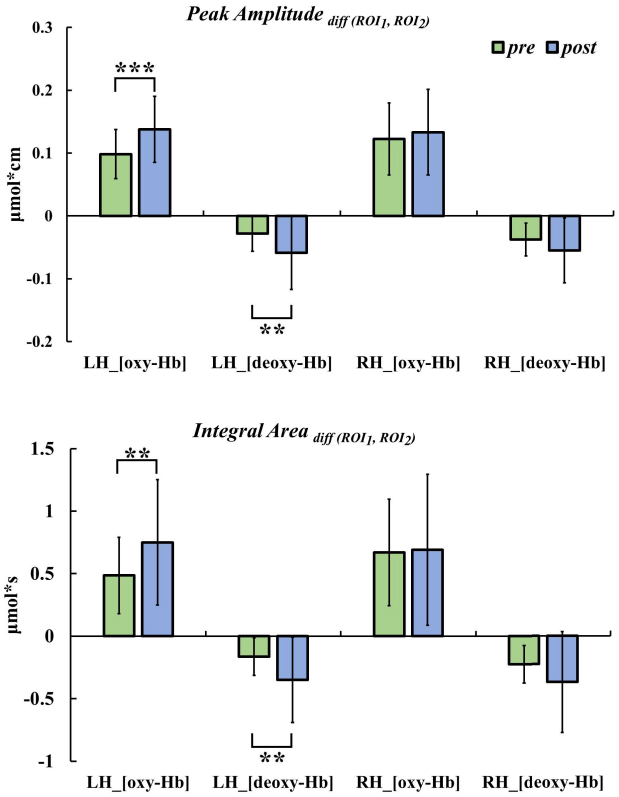

Fig. 7. MI induced cerebral blood oxygen of left- and right- hand before and after NFT. The bars represent mean value with standard error. Statistical significance has three levels (i.e. *p<0.05, **p<0.01 and ***p<0.001) according to paired-samples t-test.

the cerebral blood oxygen response of left- and right-hand MI before and after training. As shown in Fig. 8, ROI_1 and ROI_2 covered the sensorimotor regions of the brain. We calculated the mean cerebral blood oxygen concentrations induced by LH- and RH-MI and their differences. The color represents the cerebral blood oxygen concentration level. Regions in red display increased concentrations of cerebral blood oxygen ([oxy-Hb]) during MI, and blue indicates regions showing reduced concentrations of cerebral blood oxygen during MI. The results were relatively consistent with EEG activations of the sensorimotor cortex, illustrating that cortical activations induced by LH- and RH-MI were indeed significantly enhanced after transient NFT.

The topological results of cerebral blood oxygen response analysis could further verify that BCI-based visual-haptic NFT might effectively enhance MI-induced activation of hemodynamics, i.e., sensorimotor cortex, which is expected to provide a reliable assessment criterion and method for motor rehabilitation training and neural plasticity mechanism research.

D. Feature Fusion Based BCI Performance

Sixteen healthy subjects participated in the EEG-fNIRS combined collection experiment. In the classification study, we used classical CSP and SVM to calculate the classification accuracy of left- and right-hand MI before and after NFT. Fig. 9 shows the classification accuracy under different data conditions before and after NFT. Different color bars represent different data conditions (fNIRS, EEG and Hybrid) with their respective standard errors. We applied two and one-way repeated measures analysis of variance (ANOVA) to perform statistical tests. The black dashed line represents the 70% acceptable classification accuracy threshold [38]. Statistical results based on two-way ANOVA that there was no interaction between different classification methods (EEG, fNIRS and Hybrid conditions) and changes of *pre*- and *post*-NFT (F (2, 30) = 0.229, p = 0.797 > 0.05), their interactive item was not violated sphericity according to Mauchly's Test of Sphericity (χ^2 =1.513, p = 0.469), and they both had an impact on the classification accuracy respectively (Before and after training: F (1, 15) = 45.575, p = 0.000< 0.001; Different classification methods: F (2, 30) = 38.347, p = 0.000 < 0.001). The statistical results were further refined in the follow-up according to one-way ANOVA and its pairwise comparison.

Classification accuracies of different data before NFT are relatively low in most subjects. Most are below 70%, and the independent data mode is even higher than chance level (50%). After applying feature fusion by splicing EEG and fNIRS CSP vectors only, the average classification accuracy was 76.63% over all subjects. ANOVA yielded that Huynh-Feldt should be used for correction after the Mauchly's Test of Sphericity (ε = 0.931>0.75, Maxwell & Delaney, 2004), and this classification performance was significantly higher than that of single EEG or fNIRS (fNIRS: 64.69% and EEG: 71.09%, F (1.862, 27.923) = 39.845, p = 0.000 < 0.001). In addition, the Bonferroni post hoc test also yielded that the classification performance under hybrid feature fusion of EEG and fNIRS was significantly higher than that of single EEG or fNIRS with pairwise comparisons (*Hybrid-pre vs. fNIRS-pre*: p = 0.000, *Hybrid-pre vs. EEG-pre:* p=0.000).

Classification accuracies after NFT are apparently higher than those before NFT. The classification accuracies of most subjects were above 70%, which might be due to the transient NFT. In addition, the average classification accuracy reached 84.45% under the feature fusion condition over all subjects, which was significantly higher than that of single EEG or fNIRS (fNIRS: 70.78% and EEG: 79.43%; ANOVA: F (2, 30) = 17.919, p = 0.000 < 0.001). Bonferroni post hoc test also yielded classification performance under hybrid feature fusion of EEG and fNIRS is significantly higher than that of single EEG or fNIRS with pairwise comparisons (*Hybrid-pre vs. fNIRS-pre:* p=0.001, *Hybrid-pre vs. EEG-pre:* p=0.000). These results revealed that EEG-fNIRS feature fusion could optimize the performance of MI-BCI after the transient visual-haptic NFT.

E. WENP Based BCI Performance

Table I shows the comparison of MI-BCI classification performance under two different fusion methods. The average classification accuracy of all subjects increased from 84.45% to 89.14%. The Shapiro–Wilk test indicated that the classification accuracy data were normally distributed across all subjects. The paired-samples t test yielded a significant difference in classification performance between the two different fusion methods (t(15)=−3.97, p = 0.001, d = −0.99). These

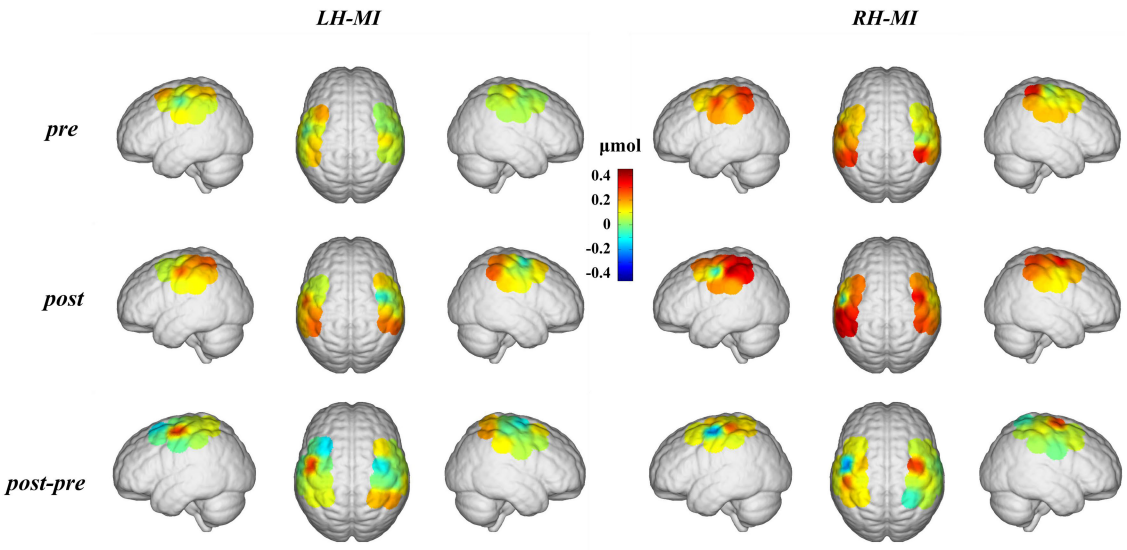

Fig. 8. The topology of the cerebral blood oxygen response induced by left- and right-hand MI (LH-MI and RH-MI) before and after NFT.

TABLE I
ALL SUBJECTS AND THEIR AVERAGE CLASSIFICATION ACCURACY OF CLASSIFICATION PERFORMANCE UNDER DIFFERENT FUSION METHODS

Subjects	**Classification Accuracy (%)**		
	Feature fusion	*Decision fusion*	*Difference (diff)*
S1	100.00	100.00	0.00
S2	82.50	85.50	3.00
S3	95.00	92.60	-2.40
S4	72.50	85.70	13.20
S5	87.50	87.00	-0.50
S6	87.50	92.50	5.00
S7	82.50	94.80	12.30
S8	90.00	94.40	4.40
S9	82.50	89.90	7.40
S10	86.88	89.20	2.32
S11	81.25	84.50	3.25
S12	75.62	87.80	12.18
S13	81.25	86.50	5.25
S14	83.75	85.10	1.35
S15	77.50	78.80	1.30
S16	85.00	91.90	6.90
Mean	84.45	89.14	4.68
Std.	6.88	5.11	4.70

results demonstrate that compared with feature fusion, our decision fusion method, WENP, could significantly improve the performance of MI-BCI.

IV. DISCUSSION

In this work, MI-BCI based NFT has shown effective prospects in motor rehabilitation. According to our fNIRS data analysis, the cerebral blood oxygen response indeed increased after this transient NFT, which is consistent with our previous study [34]. Theoretically, neural activation requires oxygen supply from the brain blood [39], [40]. Additionally, we found typical cortical activations, increasing in [oxy-Hb] and decreasing in [deoxy-Hb] during MI [41]. During motor training in clinical applications, MI performance is subjective and unstable and difficult to improve, unlike motor execution. Moreover, there is a lack of targeted evaluation criteria. All of these factors limit the application of MI- or MI-BCI-related clinical rehabilitation. As shown in Fig. 6-8, both EEG and cerebral blood oxygen activation induced by the MI response were consistently enhanced after transient visual-haptic NFT. Specifically, fNIRS results (peak amplitude, integral area, topological analysis) verified its promising effectiveness in motor rehabilitation. These EEG and fNIRS patterns might also provide a possible method of improving MI performance and cortical assessment of motor training.

Both EEG- or fNIRS-based classification performance was enhanced after NFT, which is consistent with our previous study [34]. Volunteers with lower accuracy before NFT could enhance their cortical activations during BCI training. However, previous studies have rarely determined the effects of BCI training on classification accuracy, especially based on multimodal brain imaging information [35]. Our study revealed that transient NFT might improve MI-BCI performance. More importantly, we integrated EEG and fNIRS patterns, resulting in more cortical information and better classification. Specifically, from Fig. 9, the fNIRS-based classification results are always poorer than those of EEG. First, fNIRS patterns induced by single trial MI are relatively weak and not as strong as those induced by EEG, leading to a poor initialized classification performance. Second, the strongest fNIRS pattern might generally lag behind the MI task period. Fig. 5 and 6 show that concentration changes in cerebral blood oxygen usually reach a peak in 5 seconds or even longer after task stimulus [42], [43]. However, we only take the task period data, consistent with EEG data, to perform classification.

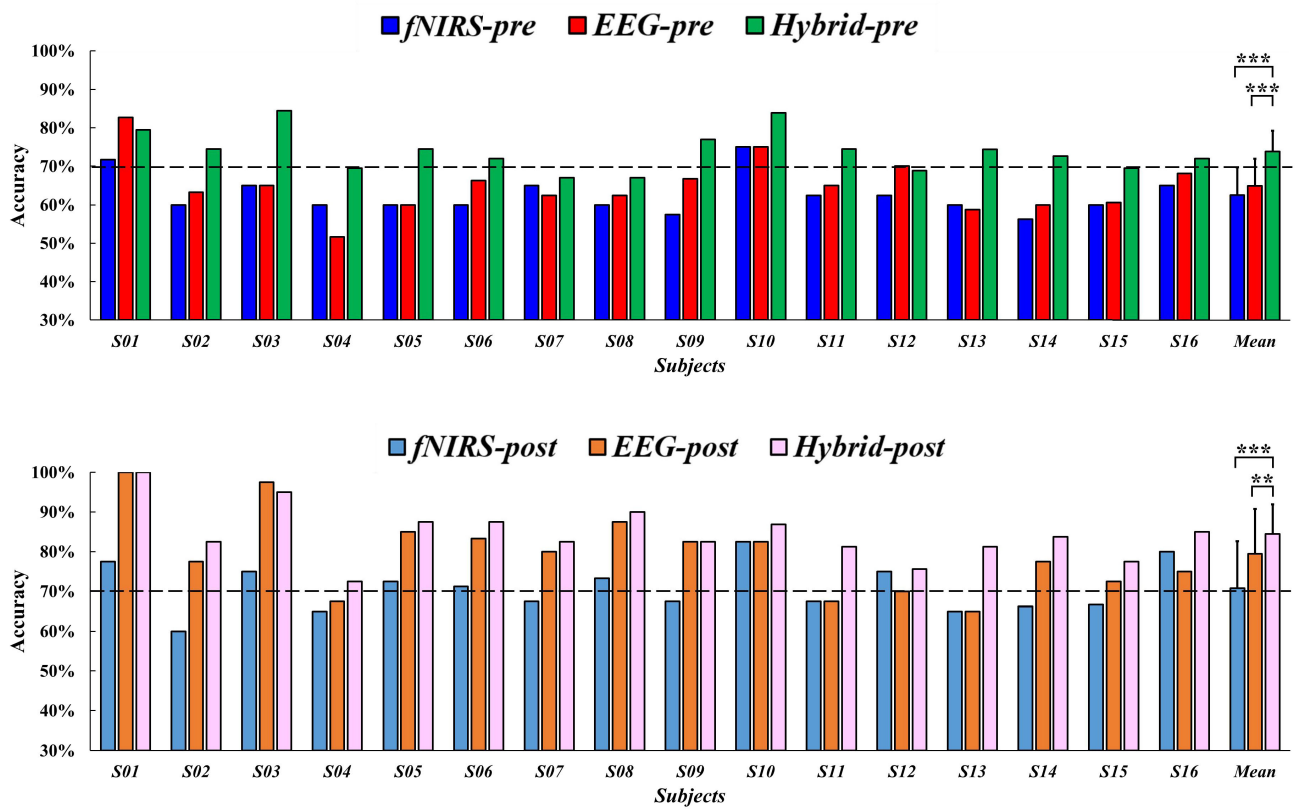

Fig. 9. All subjects and their average classification accuracy of different data or combinations during previous and posterior control sessions. (* represents the significant difference, *p < 0.05, **p < 0.01 and ***p < 0.001). The black dashed line indicates acceptable BCI performance in 70%.

fNIRS patterns of cerebral blood oxygen changes contain relatively precise spatial information and differ from EEG patterns. EEG recording has a high temporal resolution and relatively low spatial resolution [44], [45], [46]. Theoretically, hybrid data fusion could realize information compensation to improve classification performance [47], [48]. For both feature and decision fusion, the average classification accuracy is significantly increased relative to that of independent data. To some extent, this result confirms the effectiveness of information complementation. Many previous studies have supported this idea [31], [49], [50]. In addition, we compared different data fusion methods to optimize BCI performance, in which decision-level fusion (WENP) shows a better performance and effective strategy for the BCI setup.

From Fig. 9, some subjects (e.g., *pre*: S04, S07, and S13; *post*: S12) showed different results in that fNIRS accuracy was higher than EEG accuracy. This might be due to individual differences. A previous study also determined that approximately 15% to 30% of subjects have poor performance in controlling BCI [51]. Not everyone performs well with only a certain brain signal. The fusion of multiple data sets could construct the most appropriate and robust BCI classifier. From table I, decision fusion (i.e., WENP) works better according to the average classification performance. Theoretically, decision fusion uses weight assessment to better reduce the effect of misclassification than feature fusion, which does less for fault tolerance [52]. Feature fusion contains more complex information than decision fusion, which might influence the classification results. In this work, all the fusion methods we used are simple ones with some limitations (e.g., propriety of weight parameters). However, simple methods have even obtained higher accuracy than previous studies [53], which might be due to different data structures and classification strategies. In addition, we also conducted a multi-way repeated measures ANOVA, but didn't get consistent results.

We explore an offline optimized strategy to improve BCI performance, whether incorporation of EEG-fNIRS or NFT paradigms. The classification data epochs were extracted from 0.5 to 3.5 s of each MI trial under a multichannel EEG and fNIRS synchronous acquisition platform. We tried to use a longer data epoch for additional analysis under the current data set, which showed a better BCI performance. When the hybrid EEG-fNIRS classifier was fed with the full 15 s trial data, the average classification accuracy reached over 90%. We might need to design a well-designed online BCI experiment and compare differences by applying full trial data or not and determine the possible decoding speed/accuracy. Specifically, an obvious concern is the time delay of the hemodynamic response under the fNIRS system compared with the general EEG-based BCI [29], [54]. It is valuable and important to explore the combination and discrimination of different signal features to further improve the BCI classification performance [55], [56]. As shown in Fig. 10, different feature selections and combinations achieve different visual discrimination results. Alpha and beta band ERD combined with peak amplitude could give a more obvious discrimination

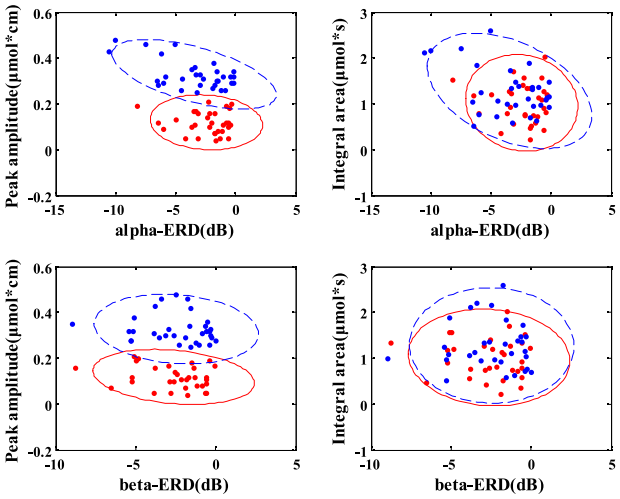

Fig. 10. Distributions of two classes MI induced ERD and cerebral blood oxygen features. The features of left and right hand motor imagery are marked by the red and blue dots, respectively. The features were plotted after normalization.

than that with integral area of cerebral blood oxygen. This seemed to contradict the results in Fig. 7, mainly due to the small amount of data. In addition, the inseparability of ERD features did not mean that EEG could not classify hand MI under CSP conditions. The results of Fig. 10 could be extended to further optimize and improve performance of MI or even other paradigm-based BCI.

Multiple data fusion technologies could achieve a positive effect on BCI performance improvement. In this study, we proposed two kinds of data fusion methods. In the future, we could probe more superior approaches with multiple data patterns to realize higher BCI classification accuracy. More real-time BCI experiments and advanced adaptive feature sets are possible and necessary to achieve an optimal combined system. Alternatively, even a zero-training classifier could be probed and contribute to building the ideal BCI paradigm. A further interesting aspect that is not limited to fNIRS and EEG patterns is that it could study the nonstationarity of multi-data during a motor training of short- or long-term. For the improvement of MI-BCI performance, it was relatively sufficient to compare the previous and posterior control sessions, although no control group was set. For future research, a control group might be necessary to further optimize the NFT framework and validate its superiority. However, it also remains unclear whether specific neural mechanisms (such as region-specific facilitation or neural plasticity) have been occurred to explain these results comprehensively.

V. Conclusion

In this study, the EEG characteristics (absolute ERD power, etc.) and cerebral blood oxygen response (concentration time course waveform peak amplitude, integral area, spatial topology, etc.) induced by MI before and after NFT were analyzed. The results revealed that EEG and fNIRS detected the same trend in motor cortex region: cortical excitability was enhanced after transient visual-haptic NFT, which is promising evidence and a feasible assessment method for motor training and rehabilitation. Additionally, EEG and fNIRS data fusion shows superior classification performance. In addition, decision fusion (i.e., WENP) is an effective classifier calibration strategy to improve the MI-BCI performance and could also be applied to other BCI paradigms. Although the real-time quantitative evaluation of neural feedback information is greatly affected by the dimension of information features and individual differences, these findings validate that our proposed fusion and assessment methods are feasible and promising for optimizing conventional motor training methods and clinical rehabilitation.

Acknowledgment

The authors sincerely thank all participants for their voluntary participation.

References

[1] F. Pichiorri et al., "Brain–computer interface boosts motor imagery practice during stroke recovery," *Ann. Neurol.*, vol. 77, no. 5, pp. 851–865, May 2015.

[2] S. C. Cramer et al., "Harnessing neuroplasticity for clinical applications," *Brain*, vol. 134, no. 6, pp. 1591–1609, 2011.

[3] M. Ietswaart et al., "Mental practice with motor imagery in stroke recovery: Randomized controlled trial of efficacy," *Brain*, vol. 134, no. 5, pp. 1373–1386, May 2011.

[4] M. A. Dimyan and L. G. Cohen, "Neuroplasticity in the context of motor rehabilitation after stroke," *Nature Rev. Neurol.*, vol. 7, no. 2, pp. 76–85, Feb. 2011.

[5] W. Tam, K. Tong, F. Meng, and S. Gao, "A minimal set of electrodes for motor imagery BCI to control an assistive device in chronic stroke subjects: A multi-session study," *IEEE Trans. Neural Syst. Rehabil. Eng.*, vol. 19, no. 6, pp. 617–627, Dec. 2011.

[6] M. Takahashi et al., "Event related desynchronization-modulated functional electrical stimulation system for stroke rehabilitation: A feasibility study," *J. Neuroeng. Rehabil.*, vol. 9, no. 1, pp. 1–6, Dec. 2012.

[7] B. M. Young et al., "Changes in functional brain organization and behavioral correlations after rehabilitative therapy using a brain–computer interface," *Frontiers Neuroeng.*, vol. 7, p. 26, Jul. 2014.

[8] C. Tangwiriyasakul, V. Mocioiu, M. J. A. M. van Putten, and W. L. C. Rutten, "Classification of motor imagery performance in acute stroke," *J. Neural Eng.*, vol. 11, no. 3, Jun. 2014, Art. no. 036001.

[9] V. Kaiser, A. Kreilinger, G. R. Müller-Putz, and C. Neuper, "First steps toward a motor imagery based stroke BCI: New strategy to set up a classifier," *Frontiers Neurosci.*, vol. 5, p. 86, Jan. 2011.

[10] A. Ramos-Murguialday et al., "Brain–machine interface in chronic stroke rehabilitation: A controlled study," *Ann. Neurol.*, vol. 74, no. 1, pp. 100–108, Jul. 2013.

[11] K. K. Ang et al., "Facilitating effects of transcranial direct current stimulation on motor imagery brain-computer interface with robotic feedback for stroke rehabilitation," *Arch. Phys. Med. Rehabil.*, vol. 96, no. 3, pp. S79–S87, Mar. 2015.

[12] W. Teo and E. Chew, "Is motor-imagery brain–computer interface feasible in stroke rehabilitation?" *PM&R*, vol. 6, no. 8, pp. 723–728, Aug. 2014.

[13] R. Rupp, "Challenges in clinical applications of brain computer interfaces in individuals with spinal cord injury," *Frontiers Neuroeng.*, vol. 7, p. 38, Jun. 2014.

[14] K. Nakayashiki, M. Saeki, Y. Takata, Y. Hayashi, and T. Kondo, "Modulation of event-related desynchronization during kinematic and kinetic hand movements," *J. Neuroeng. Rehabil.*, vol. 11, no. 1, pp. 1–9, Dec. 2014.

[15] S. Aydin, "Deep learning classification of neuro-emotional phase domain complexity levels induced by affective video film clips," *IEEE J. Biomed. Health Informat.*, vol. 24, no. 6, pp. 1695–1702, Jun. 2020.

[16] S. Aydın, "Cross-validated Adaboost classification of emotion regulation strategies identified by spectral coherence in resting-state," *Neuroinformatics*, vol. 20, no. 3, pp. 1–13, 2021.

[17] W. Yi, S. Qiu, H. Qi, L. Zhang, B. Wan, and D. Ming, "EEG feature comparison and classification of simple and compound limb motor imagery," *J. Neuroeng. Rehabil.*, vol. 10, no. 1, pp. 1–12, Dec. 2013.

[18] B. Blankertz, R. Tomioka, S. Lemm, M. Kawanabe, and K.-R. Müller, "Optimizing spatial filters for robust EEG single-trial analysis," *IEEE Signal Process. Mag.*, vol. 25, no. 1, pp. 41–56, Jun. 2008.

[19] R. Sitaram et al., "Closed-loop brain training: The science of neurofeedback," *Nature Rev. Neurosci.*, vol. 18, no. 2, pp. 86–100, Feb. 2017.

[20] U. Chaudhary, N. Birbaumer, and A. Ramos-Murguialday, "Brain–computer interfaces for communication and rehabilitation," *Nature Rev. Neurol.*, vol. 12, no. 9, pp. 513–525, 2016.

[21] A. Abdalmalak et al., "Assessing time-resolved fNIRS for brain–computer interface applications of mental communication," *Frontiers Neurosci.*, vol. 14, p. 105, Feb. 2020.

[22] E.-M. Kurz et al., "Towards using fNIRS recordings of mental arithmetic for the detection of residual cognitive activity in patients with disorders of consciousness (DOC)," *Brain Cognition*, vol. 125, pp. 78–87, Aug. 2018.

[23] F. Biessmann, S. Plis, F. C. Meinecke, T. Eichele, and K. Müller, "Analysis of multimodal neuroimaging data," *IEEE Rev. Biomed. Eng.*, vol. 4, pp. 26–58, 2011.

[24] Y. Murayama et al., "Relationship between neural and hemodynamic signals during spontaneous activity studied with temporal kernel CCA," *Magn. Reson. Imag.*, vol. 28, no. 8, pp. 1095–1103, Oct. 2010.

[25] T. Grossmann, R. Oberecker, S. P. Koch, and A. D. Friederici, "The developmental origins of voice processing in the human brain," *Neuron*, vol. 65, no. 6, pp. 852–858, Mar. 2010.

[26] J. Sui, T. Adali, Q. Yu, J. Chen, and V. D. Calhoun, "A review of multivariate methods for multimodal fusion of brain imaging data," *J. Neurosci. Methods*, vol. 204, no. 1, pp. 68–81, Feb. 2012.

[27] C. Han, K. Müller, and H. Hwang, "Enhanced performance of a brain switch by simultaneous use of EEG and NIRS data for asynchronous brain–computer interface," *IEEE Trans. Neural Syst. Rehabil. Eng.*, vol. 28, no. 10, pp. 2102–2112, Oct. 2020.

[28] B. Koo et al., "A hybrid NIRS-EEG system for self-paced brain computer interface with online motor imagery," *J. Neurosci. Methods*, vol. 244, pp. 26–32, Apr. 2015.

[29] Y. Tomita, F.-B. Vialatte, G. Dreyfus, Y. Mitsukura, H. Bakardjian, and A. Cichocki, "Bimodal BCI using simultaneously NIRS and EEG," *IEEE Trans. Biomed. Eng.*, vol. 61, no. 4, pp. 1274–1284, Apr. 2014.

[30] L. Kauhanen et al., "EEG and MEG brain–computer interface for tetraplegic patients," *IEEE Trans. Neural Syst. Rehabil. Eng.*, vol. 14, no. 2, pp. 190–193, Jun. 2006.

[31] S. Fazli et al., "Enhanced performance by a hybrid NIRS–EEG brain computer interface," *NeuroImage*, vol. 59, no. 1, pp. 519–529, Jan. 2012.

[32] A. P. Buccino, H. O. Keles, and A. Omurtag, "Hybrid EEG-fNIRS asynchronous brain–computer interface for multiple motor tasks," *PloS One*, vol. 11, no. 1, 2016, Art. no. e0146610.

[33] A. M. Chiarelli et al., "Simultaneous functional near-infrared spectroscopy and electroencephalography for monitoring of human brain activity and oxygenation: A review," *Neurophotonics*, vol. 4, no. 4, 2017, Art. no. 041411.

[34] Z. Wang et al., "A BCI based visual-haptic neurofeedback training improves cortical activations and classification performance during motor imagery," *J. Neural Eng.*, vol. 16, no. 6, Oct. 2019, Art. no. 066012.

[35] V. Kaiser et al., "Cortical effects of user training in a motor imagery based brain–computer interface measured by fNIRS and EEG," *NeuroImage*, vol. 85, pp. 432–444, Jan. 2014.

[36] G. R. Müller-Putz, I. Daly, and V. Kaiser, "Motor imagery-induced EEG patterns in individuals with spinal cord injury and their impact on brain–computer interface accuracy," *J. Neural Eng.*, vol. 11, no. 3, Jun. 2014, Art. no. 035011.

[37] Z. Wang et al., "BCI monitor enhances electroencephalographic and cerebral hemodynamic activations during motor training," *IEEE Trans. Neural Syst. Rehabil. Eng.*, vol. 27, no. 4, pp. 780–787, Apr. 2019.

[38] B. Z. Allison, C. Brunner, V. Kaiser, G. R. Müller-Putz, C. Neuper, and G. Pfurtscheller, "Toward a hybrid brain–computer interface based on imagined movement and visual attention," *J. Neural Eng.*, vol. 7, no. 2, Apr. 2010, Art. no. 026007.

[39] C. Roy and C. Sherrington, "On the regulation of the blood-supply of the brain," *J. Physiol.*, vol. 11, nos. 1–2, pp. 85–158, 1890.

[40] Y. Ota et al., "Motor imagery training with neurofeedback from the frontal pole facilitated sensorimotor cortical activity and improved hand dexterity," *Frontiers Neurosci.*, vol. 14, p. 34, Jan. 2020.

[41] I. Vanzetta and A. Grinvald, "Coupling between neuronal activity and microcirculation: Implications for functional brain imaging," *HFSP J.*, vol. 2, no. 2, pp. 79–98, Apr. 2008.

[42] R. B. Buxton et al., "Modeling the hemodynamic response to brain activation," *NeuroImage*, vol. 23, pp. 220–233, Jan. 2004.

[43] A. R. Mayer, T. Toulouse, S. Klimaj, J. M. Ling, A. Pena, and P. S. F. Bellgowan, "Investigating the properties of the hemodynamic response function after mild traumatic brain injury," *J. Neurotrauma*, vol. 31, no. 2, pp. 189–197, Jan. 2014.

[44] J.-P. Lachaux, E. Rodriguez, J. Martinerie, and F. J. Varela, "Measuring phase synchrony in brain signals," *Hum. Brain Mapping*, vol. 8, no. 4, pp. 194–208, 1999.

[45] J.-M. Schoffelen and J. Gross, "Source connectivity analysis with MEG and EEG," *Hum. Brain Mapping*, vol. 30, no. 6, pp. 1857–1865, Jun. 2009.

[46] V. Quaresima, S. Bisconti, and M. Ferrari, "A brief review on the use of functional near-infrared spectroscopy (fNIRS) for language imaging studies in human newborns and adults," *Brain Lang.*, vol. 121, no. 2, pp. 79–89, May 2012.

[47] P. A. Cicalese et al., "An EEG-fNIRS hybridization technique in the four-class classification of Alzheimer's disease," *J. Neurosci. Methods*, vol. 336, Apr. 2020, Art. no. 108618.

[48] Y. Fu, X. Xiong, C. Jiang, B. Xu, Y. Li, and H. Li, "Imagined hand clenching force and speed modulate brain activity and are classified by NIRS combined with EEG," *IEEE Trans. Neural Syst. Rehabil. Eng.*, vol. 25, no. 9, pp. 1641–1652, Sep. 2017.

[49] F. Putze et al., "Hybrid fNIRS-EEG based classification of auditory and visual perception processes," *Frontiers Neurosci.*, vol. 8, p. 373, Nov. 2014.

[50] X. Yin et al., "A hybrid BCI based on EEG and fNIRS signals improves the performance of decoding motor imagery of both force and speed of hand clenching," *J. Neural Eng.*, vol. 12, no. 3, Jun. 2015, Art. no. 036004.

[51] A. Nijholt and D. Tan, "Brain–computer interfacing for intelligent systems," *IEEE Intell. Syst.*, vol. 23, no. 3, pp. 72–79, May 2008.

[52] R. A. Heckemann, J. V. Hajnal, P. Aljabar, D. Rueckert, and A. Hammers, "Automatic anatomical brain MRI segmentation combining label propagation and decision fusion," *NeuroImage*, vol. 33, no. 1, pp. 115–126, Oct. 2006.

[53] J. Kwon, J. Shin, and C.-H. Im, "Toward a compact hybrid brain-computer interface (BCI): Performance evaluation of multi-class hybrid EEG-fNIRS BCIs with limited number of channels," *PLoS ONE*, vol. 15, no. 3, Mar. 2020, Art. no. e0230491.

[54] J. Shin, J. Kwon, and C.-H. Im, "A ternary hybrid EEG-NIRS brain–computer interface for the classification of brain activation patterns during mental arithmetic, motor imagery, and idle state," *Frontiers Neuroinform.*, vol. 12, p. 5, Feb. 2018.

[55] M. Arvaneh, C. Guan, K. Keng Ang, and C. Quek, "Optimizing spatial filters by minimizing within-class dissimilarities in electroencephalogram-based brain–computer interface," *IEEE Trans. Neural Netw. Learn. Syst.*, vol. 24, no. 4, pp. 610–619, Apr. 2013.

[56] H. Zeng and A. Song, "Optimizing single-trial EEG classification by stationary matrix logistic regression in brain–computer interface," *IEEE Trans. Neural Netw. Learn. Syst.*, vol. 27, no. 11, pp. 2301–2313, Nov. 2016.